https://doi.org/10.32604/zkg.2024.01.02

Sulfate resistance of alkali-activated slag/metakaolin/fly ash cementitious materials

Junpeng Mei[1,2,3], Chong Yuan[1], Yinlong Niu[4], Jielin Zhang[1], Shuang Li[1], Hainan Li[5]
[1] School of Urban Construction, Wuhan University of Science and Technology, Wuhan/China
[2] Hubei Provincial Engineering Research Center of Urban Regeneration, Wuhan/China
[3] Institute of High Performance Engineering Structure, Wuhan University of Science and Technology, Wuhan/China
[4] China Construction Third Bureau First Engineering Co., Ltd., Wuhan/China
[5] Department of Construction Cost, Wuhan Textile University, Wuhan/China

ABSTRACT Fly ash, slag powder, and metakaolin were used as the main raw materials to prepare the ternary alkali-activated cementitious materials, and the compound alkali-activated cementitious materials with different proportions were corroded in 5% $(NH_4)_2SO_4$ solution for 120 d by different immersion methods to study their sulfate resistance. Then X-ray diffraction (XRD) and scanning electron microscopy (SEM) were used to analyze the erosion mechanism of alkali-activated cementitious materials with different mix ratios. Results show that the alkali-activated cementitious material containing 50% slag powder, 25% fly ash and 25% metakaolin shows the best sulfate resistance in $(NH_4)_2SO_4$ solution and the alkali-activated cementitious material with 60% slag powder, 28% metakaolin and 12% fly ash has the worst corrosion resistance. XRD and SEM analysis confirms the existence of gypsum phase in alkali-activated cementitious materials specimens when exposed to ammonium sulfate, indicating that chemical erosion damage occurs in the interior. These results are expected to provide reference for the theoretical research and practical application of alkali-activated cementitious materials.

MATERIALS

1 Introduction

Alkali-activated cementitious material, which is prepared with a large amount of industrial solid waste and alkaline activator according to a certain ratio, is a new building material with simple production process and low cost. It can not only provide an economic and efficient method for the recycling of large industrial solid waste, reduce its impact on the environment, but also play a role in construction and roads fields to reduce unsustainable resource consumption, with huge environmental, economic, and social benefits, and is one of the main alternatives to silicate cement in the future.

Sulfate erosion is one of the important factors affecting the durability of building materials. According to research findings, the sulfate resistance of alkali-activated cementing material was significantly higher than that of Portland cement [1-3], and the specimens prepared with low calcium system such as metakaolin had better sulfate resistance [4, 5]. Ismail et al. [6] studied the properties of alkali-activated fly ash-slag base polymers exposed to sulfate and found that gypsum formation was observed in $MgSO_4$ erosion solution, and Mg^{2+} in the solution caused decalcification of the alkali-activated cementitious system, so obvious physical deterioration could be observed in the $MgSO_4$ solution. The study of Atahan et al. [7] pointed out that the use of low-calcium mineral admixtures can significantly improve the anti-sulfate corrosion performance of the cementitious system. The results of Irassar [8] et al. showed that the incorporation of fly ash can improve the anti-erosion effect of specimens fully buried in sulfate soil, but also cause more serious exfoliation phenomenon in the air. Zheng et al. [9] found that the "wick effect" accelerated the migration of corrosive ions under the condition of semi-immersion, and the mekaoline- based mortar had excellent sulfate erosion resistance. The study of Nuaklong et al. [10] proved that the incorporation of an appropriate amount of metakaolin into the high-calcium fly ash geopymers can significantly improve the mechanical properties of concrete, make its microstructure more compact, and thus improve the sulfate corrosion resistance of the material.

Based on previous studies, it can be found that alkali-activated cementitious materials under the binary system have their own advantages. Although the mechanical properties of the fly ashslag system are better, the resistance to sulfate attack still lags behind that of the metakaolin-slag system. At present, many scholars have studied the sulfate resistance of the binary alkali-activated cementitious material system, but the research in the ternary system needs to be supplemented. Based on this, this paper studied the corrosion resistance of alkali-activated cementitious materials of the ternary system under different soaking methods to be ammonium sulfate solution

and analysed the sulfate erosion mechanism combined with the changes in mass, appearance, phase composition and apparent morphology, in order to provide support for the application of alkali-activated cementitious materials.

2 Experiment

2.1 Raw materials

The chemical compositions of fly ash (FA), metakaolin (MK) and slag powder (SP) are shown in Table 1. The sodium silicate with the modulus of 2.3 is produced from Yourui Refractory Co., Ltd and its chemical composition is 29.9% SiO_2, 13.75% Na_2O and 56.35% H_2O. The water glass modulus was adjusted to 1.5 with analytical pure sodium hydroxide. The mixing water is tap water, in accordance with the relevant provisions of JGJ 63-2006 [11]. The analytical pure ammonium sulfate was used to configure the erosion solution for the whole process of sulfate attack.

2.2 Sample preparation

The water glass (modulus 1.5), fly ash, metakaolin, slag powder and water were poured into the clean blender according to the mixing ratio in Table 2 to stir evenly, and the obtained paste was poured into the mold of 40 mm x 40 mm x 160 mm, put on the shaking table to shake solid until no bubbles emerge, and then put into the standard curing box for 1 d, and then the mold was removed. The formed paste specimens were immersed in water and cured for 28 d, and then placed in water and sulfate respectively for the erosion experiment.

2.3 Test procedure

2.3.1 Sulfate immersion test

According to the GB/T 749-2008 [12] soaking corrosion resistance test method, the resistance to sulphate sulphate attack of alkali-activated cementitious paste was tested. The soaking methods for the sulfate immersion test were divided into two categories: Part of the specimen was immersed completely in sulphate solution; the other part was half-soaked in the solution, and the height from the top of the specimen to the solution surface was kept at 8 cm. The sulfate solution was replaced every other month to ensure the erosion fluid concentration.

2.3.2 Mass change rate

When the erosion time reached 48 h, the initial mass (M_0) of the specimen was measured. During the test, when the specimen reached the set age, the specimen was taken out of the soaking solution and the mass (M_n) was measured after wiping the moisture with a towel. The mass change rate (ΔM) of the specimen is shown in Formula (1):

$$\Delta M = \frac{M_n - M_0}{M_0} \times 100\ \% \tag{1}$$

2.3.3 Strength and corrosion resistance coefficient

After the erosion age reached 30 d, 60 d, 90 d and 120 d, a YAW-200/300 automatic pressure testing machine was used to measure the compressive and flexural strength of alkali-activated cementitious materials according to GB/T 17671-2021 [13]. The loading rates of compressive strength and flexural strength were 2.4 kN/s and 50 N/s, respectively. The flexural corrosion coefficient (K_f) and compressive corrosion coefficient (K_c) are calculated according to the following formulas:

$$K_f = \frac{F_c}{F_w} \tag{2}$$

$$K_c = \frac{C_c}{C_w} \tag{3}$$

Where F_c and F_w represent the flexural strengths (MP_a) of the specimens immersed in erosion solution and in water respectively to the corresponding age, respectively; C_c, C_w represent the compressive strengths (MP_a) of the specimens immersed in erosion solution and in water respectively to the corresponding age.

Table 2 **Experimental mix ratio of ternary alkali-activated cementitious materials**

Materials	SP [g]	MK [g]	FA [g]	Sodium silicate (1.5) [g]	Water [g]
A1	810	378	162	405	405
A2	810	270	270	405	405
A3	810	162	378	405	405
B1	675	472.5	202.5	405	405
B2	675	337.5	337.5	405	405
B3	675	202.5	472.5	405	405

Table 1 **Chemical composition of raw materials**

Materials	Al_2O_3	SiO_2	Fe_2O_3	Na_2O	K_2O	CaO	MgO	SO_3	LOI
FA	36.10	44.02	5.44	0.20	1.12	5.96	0.41	1.13	5.62
SP	14.73	26.83	3.29	0.15	0.45	42.76	5.74	0	6.05
MK	46.79	45.15	2.71	0.02	0.32	0.52	0.14	0.17	4.38

2.3.4 XRD

The corroded specimens reaching a certain age were broken into small pieces and immersed in anhydrous ethanol in order to stop the hydration. After they were dried in a vacuum drying oven at 40 °C, some small pieces were ground into powders in a mortar. The powders which can pass through a 200 mesh screen were used for the XRD test at a scanning rate of 8°/min with a step size of 0.02° and a 2-theta range of 10~50°.

2.3.5 SEM

The electron scanning electron microscope was used to observe the cross section morphology of cement paste in low altitude environment. Before the test, the sample should be sprayed with gold.

3 Results and discussion

3.1 Strength

The figures from Figure 1 to Figure 6 show the flexural and compressive strength changes of alkali-activated cementitious materials with different mix ratios under immersion in ammonium sulfate solution. A(B) x-H (x=1,2,3) is the half-immersion in the $(NH_4)_2SO_4$ solution group, A(B) x-A (x=1,2,3) is the all-immersion in the $(NH_4)_2SO_4$ solution group, and A(B) x-U (x=1,2,3) is the water curing group.

As for the flexural strength, it can be observed that the strength changes of other specimens except B1 under half-immersion environment are more obvious than those under all-immersion environment. In the half-immersion group, the overall change trend of flexural strength is first increasing, then decreasing and then gradually increasing. This trend occurs because the alkali-activated cementitious material is also undergoing polymerization reaction at the initial stage of erosion, and at the same time, the salt solution enters the pores of the specimen and salt crystals fill the pores, which increase its compactness. With the increase of soaking time, the effect of the resulting crystallization on the specimen gradually appears, causing the specimen to crack and eventually leading to a decrease in strength. In the later stage, crystallization is produced to fill the crack again, and the strength rises again. In the half-immersion environment, the damage is not only physical salt crystallization damage, but also serious chemical erosion damage, the influence factors are much more complex, and thus the damage is greater. Specifically, when the erosion age reaches 120 d, the specimens A1, A2, B1 and B2 under semi-immersion reach 22.8 MPa, 17.2 MPa, 17.4 MPa and 18.8 MPa respectively. In the full immersion environment, A1, A2, B1 and B2 reached 13.4 MPa, 11.8 MPa, 14 MPa and 17.3 MPa respectively. On the whole, the flexural strength of the specimens in the half-immersion environment eroded by ammonium sulfate solution increases more rapidly than that in the all-immersion environment, and the strength development of the specimens is not greatly affected by the immersion in the solution for 120 d.

As for the compressive strength, it can be observed that the strength development of B2

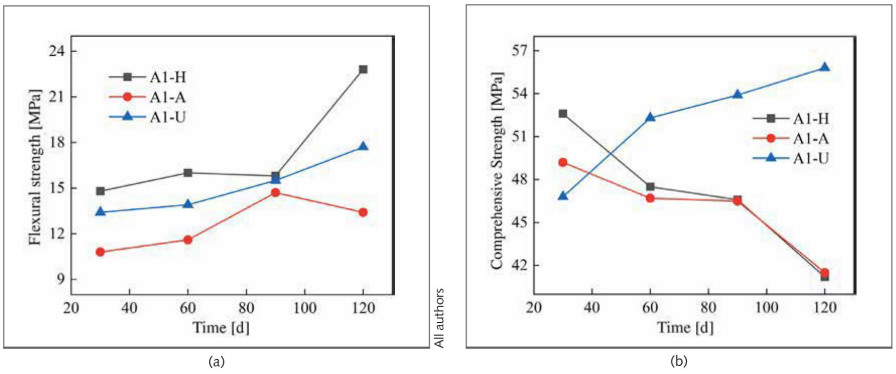

All authors

(a) (b)

1 Strength change of A1 paste immersed in sulfate solution (a) Flexural strength (b) Compressive strength

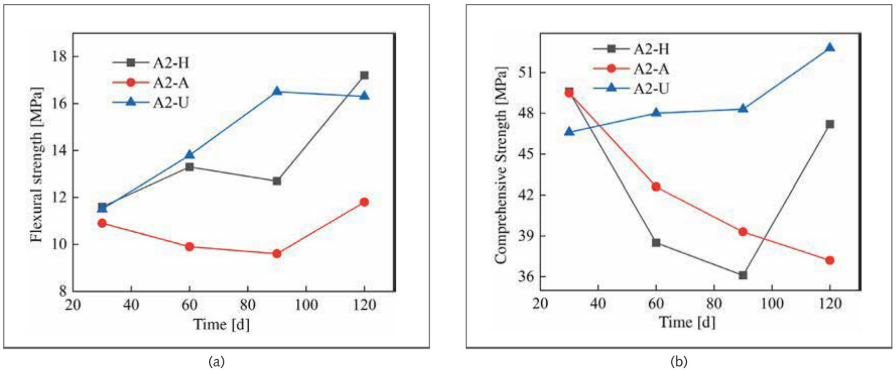

(a) (b)

2 Strength change of A2 paste immersed in sulfate solution (a) Flexural strength (b) Compressive strength

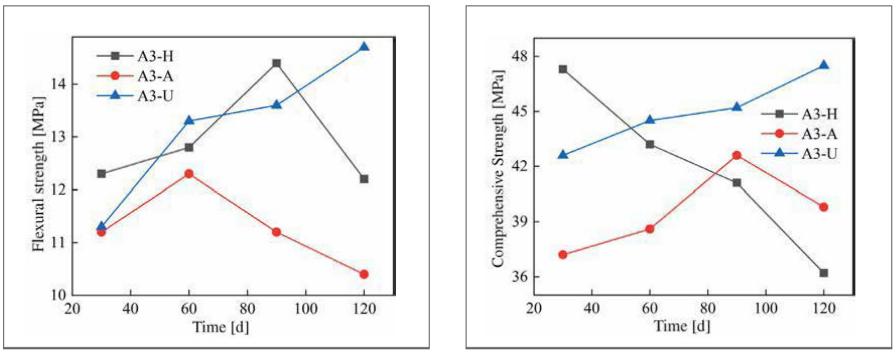

(a) (b)

3 Strength change of A3 paste immersed in sulfate solution (a) Flexural strength (b) Compressive strength

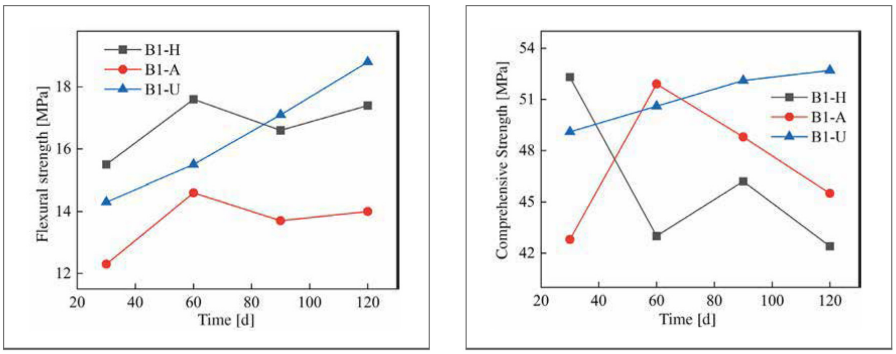

(a) (b)

4 Strength change of B1 paste immersed in sulfate solution (a) Flexural strength (b) Compressive strength

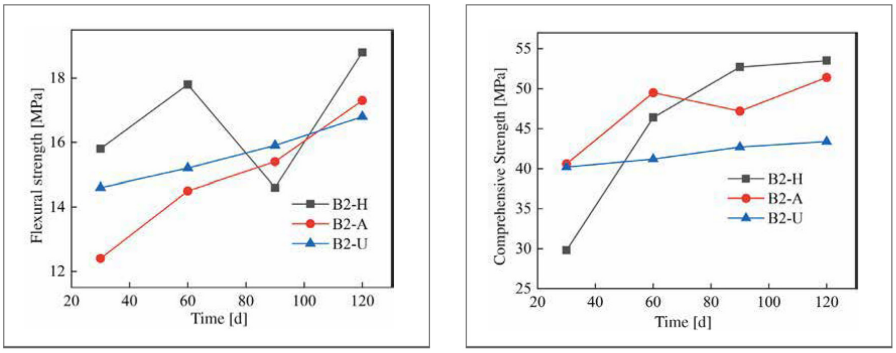

(a) (b)

5 Strength change of B2 paste immersed in sulfate solution (a) Flexural strength (b) Compressive strength

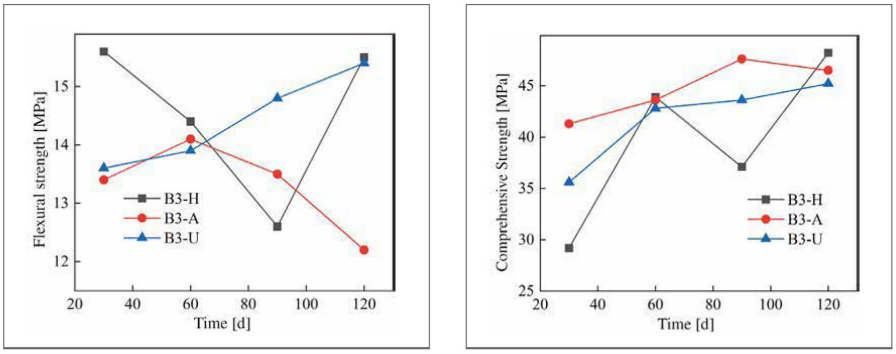

(a) (b)

6 Strength change of B3 paste immersed in sulfate solution (a) Flexural strength (b) Compressive strength

and B3 specimens in the early stage of half-immersion is inhibited. From the data of the control group, it can be found that the overall strength of ternary alkali-activated cementitious materials develops rapidly and has a high strength, and the strength grows slowly within a certain range after 30 days of water curing. At 120 d, the compressive strengths of A1, A2, A3, B1, B2 and B3 reach 41.2 MPa, 47.2 MPa, 36.2 MPa, 42.4 MPa, 53.5 MPa and 48.2 MPa respectively under half-immersion, reach 41.5 MPa, 37.2 MPa, 39.8 MPa, 45.5 MPa, 51.4 MPa and 46.5 MPa respectively under all-immersion. When the content of slag powder is 50%, the alkali-activated cementitious material shows better mechanical properties and sulfate erosion resistance as a whole, and the content of metakaolin also has an impact on the compressive strength of the specimen. It can be observed that the specimen with higher content of metakaolin shows higher mechanical properties. At 120 d, the compressive strengths of control group of A1, A2 and B1 reach 55.8 MPa, 52.8 MPa and 52.7 MPa, respectively. It is concluded that metakaolin particles are fine and have a large special surface area, so it can increase the compressive strength of the specimen and make the microstructure more compact. It can also be observed that in the all-immersion erosion environment, with the decrease of slag powder content, the anti-sulfate corrosion performance of the specimens also gradually increases, which also proves that the alkali-activated cementitious materials with low calcium or no calcium often have better anti-sulfate corrosion performance, because the high content of SiO_2 in fly ash and metakaolin can improve the C-S-H gel in concrete and affect its hardening performance [14].

3.2 Corrosion resistance coefficient

Figure 7 shows the flexural/compressive corrosion resistance coefficient of the specimens at different ratios.

Referring to the standard of cement's sulphate corrosion resistance, the flexural/compressive corrosion resistance coefficient ≥0.8 can be considered to have good sulfate corrosion resistance, while the flexural/compressive strength of the ternary system of alkali-activated cementitious materials soaking in $(NH_4)_2SO_4$ does not decrease significantly, which shows excellent sulfate corrosion resistance under the condition of half-immersion. Specially, the flexural corrosion resistance coefficients of B1, B2 and B3 are 0.92, 1.11 and 1.01 respectively, and the compressive corrosion resistance coefficients are 0.8, 1.23 and 1.06, respectively when the erosion age reaches 120 d. This may be due to the fact that the expansion stress generated by the reaction between sulfate ions infiltrating into the specimen and the specimen is not enough to cause damage to the specimen but plays a role in enhancing the flexural and compressive strength of the specimen at the current age, which indicates that the ternary alkali-activated cementitious material has good sulfate erosion resistance. The B2 specimen has the best sulfate resistance in the ternary system, and the flexural/compressive corrosion resistance coefficients are 1.03 and 1.18 in the all-immersion environment at 120 d.

3.3 Mass change rate

Figure 8 shows the mass change rate of the sample of alkali-activated slag-metakaolin-fly ash cementitious materials in ammonium sulfate solution under different soaking methods.

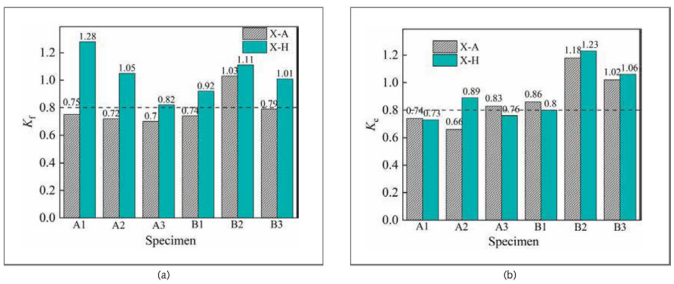

7 Flexural/compressive corrosion resistance coefficient of the ternary pastes after soaking in sulfate solution for 120 d (a) Flexural corrosion resistance coefficient (b) Compressive corrosion resistance coefficient

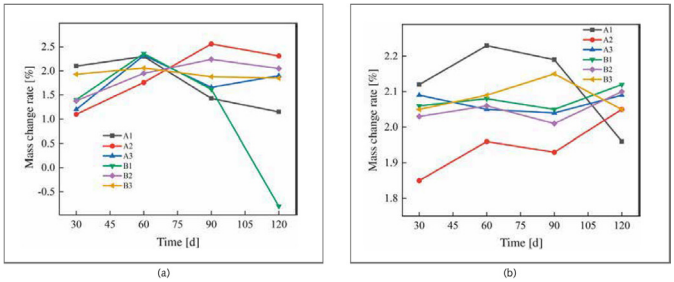

8 Mass change rate of ternary pastes soaked in sulfate solution (a) Half-immersion (b) All-immersion

As shown in Figure 8 (a), the mass of B1 sample drops by 0.8% at 120 d of erosion under the half-immersion erosion environment due to the phenomenon of large area spalling. In the other samples, there is no powder spalling phenomenon, and the overall mass change rate does not fluctuate in a wide range. It can be observed that the mass of specimens in the ternary system increases rapidly before 30 d, and A1 and B3 have the highest growth rate, which are 2.10% and 1.93% respectively at the erosion age of 30 d. However, during the 30 d to 60 d erosion age period, the growth rate remains slow, and then the mass change rate begins to decline. The mass of the A2 specimen increases steadily before 90 d of erosion age in a half-immersion environment, and then declines after 90 d. The mass change rate of the A3 specimen increases again at 90 d, which can be considered as periodic erosion failure in the interior. Other specimens do not show periodic phenomenon temporarily under half-immersion, so it can be inferred that periodic erosion failure will also appear with the extension of the test erosion age.

The mass change rate of specimens in the all-immersion erosion environment is similar to that in the half-immersion group. The masses of A2, B1 and B2 specimens show periodic changes patterns, which increase all the time before 60 d, decrease slightly from 60 d to 90 d, and begin to increase again after 90 d, B3 decreases at 90 d, and A1 decreases continuously after 60 d. Among all samples, A1 has the lowest mass change rate of 1.96% at 120 d.

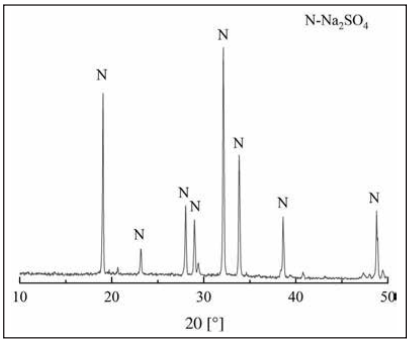

9 XRD pattern of white crystals formed on the surface of specimen immersed in sulphate solution

3.4 Erosion product analysis

The white crystal produced by the specimen in the environment of half-immersion erosion was taken for the XRD test, and the results are shown in Figure 9. It can be found that it is mainly composed of Na_2SO_4 phase, is probably made from the decomposition of $Na_2SO_4 \cdot 10H_2O$ after drying in the oven, and proves that serious physical salt crystal erosion damage occurred under half-immersion.

XRD tests were conducted on A1 and B2 samples soaked for 30 d and 120 d with all-immersion and half-immersion and were compared with water-cultured specimens of the same age to study whether alkali-activated cementitious of ternary mixture produced new hydration products under sulfate attack, as shown in Figure 10. It can be seen from Figure 10 that gypsum was produced in alkali-activated cementitious of ternary mixture under sulfate attack, and the main crystals of

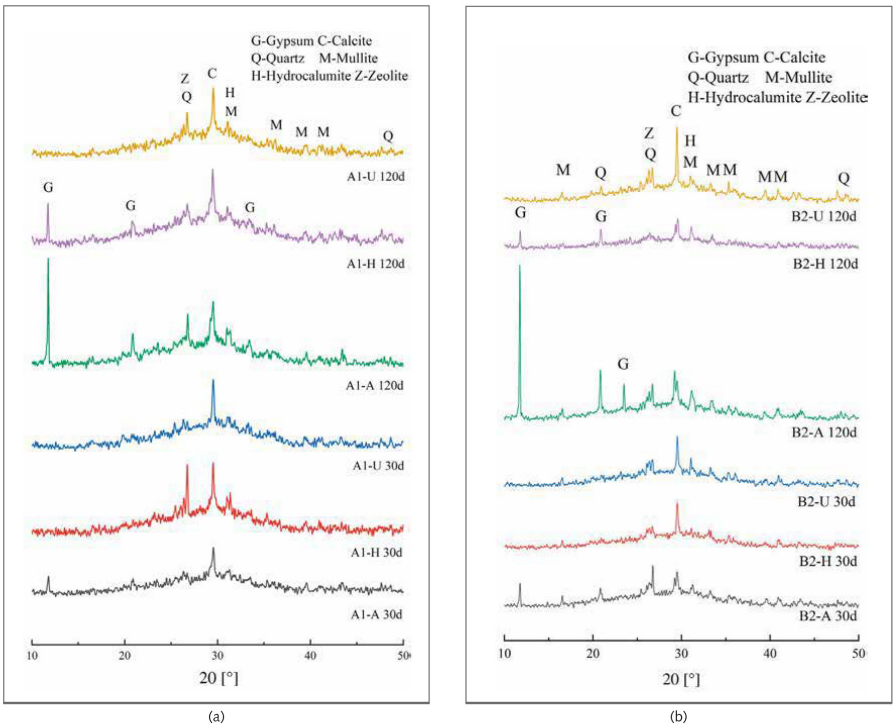

10 XRD patterns of A1 and B2 specimens immersed in sulfate solution: (a) A1; (b) B2

all samples were basically the same under different proportions, consisting of gypsum, quartz and mullite. An obvious "steamed bun peak" can also be observed at 28.5~30°, indicating the presence of an amorphous gelatinous substance, namely C-A-S-H gels. By comparing the XRD patterns of A1 and B2, it can be found that the C-A-S-H gel phase of B2 in water curing condition is significantly higher than that of A1, indicating that with the decrease of slag powder content and the increase of fly ash and metakaolinite, the calcium content in the system gradually decreases, and the secondary hydration of fly ash would consume a large amount of calcium hydroxide, resulting in an increase of C-A-S-H gels. In addition, A1 and B2 samples show obvious gypsum phase after full soaking for 120 d, which is because sulfate ions can infiltrate into the pores and react with C-A-S-H gel in the specimen to form gypsum, resulting in the reduction of compressive strength and the increase of mass of the specimens [15]. Moreover, the mullite phase does not change with the increase of erosion age, indicating that mullite has stable sulfate resistance. Therefore, it can be considered that there is not only physical salt crystallization destruction, but also chemical erosion destruction in alkali-activated cementitious of ternary mixture soaked in ammonium sulfate.

3.5 SEM analysis

Figure 11 and Figure 12 show the SEM images of A1 and B2 specimens with erosion ages of 30 d and 120 d under different soaking methods in magnesium sulfate solution.

As can be seen from Figure 11, when the erosion age is 30 d, the surface of A1 specimens under different soaking methods is covered with a large number of flocs with poor compactness. As the erosion age gradually increases to 120 d, the flocs on the surface gradually disappear and the surfaces are covered by gels. Simultaneously, lamellar products can also be observed on the surface, and the lamellar structures overlap parallel and compact in a local small range. It is believed that more C-A-S-H is generated with longer age, and C-A-S-H gel has higher spatial filling capacity than N-A-S-H gel, which can refine the porosity and improve the strength of the cementitious system. At the same time, the pore structure and the sulfate resistance of the specimen are further developed with the age, and the microstructure is more compact [16, 17].

As can be seen from Figure 12, when the erosion age is 30 d, the surface under water cultivation is covered with a large number of crystal particles, which may be calcite ($CaCO_3$) produced by carbonization. The surface of specimens under both half-immersion and all-immersion erosion

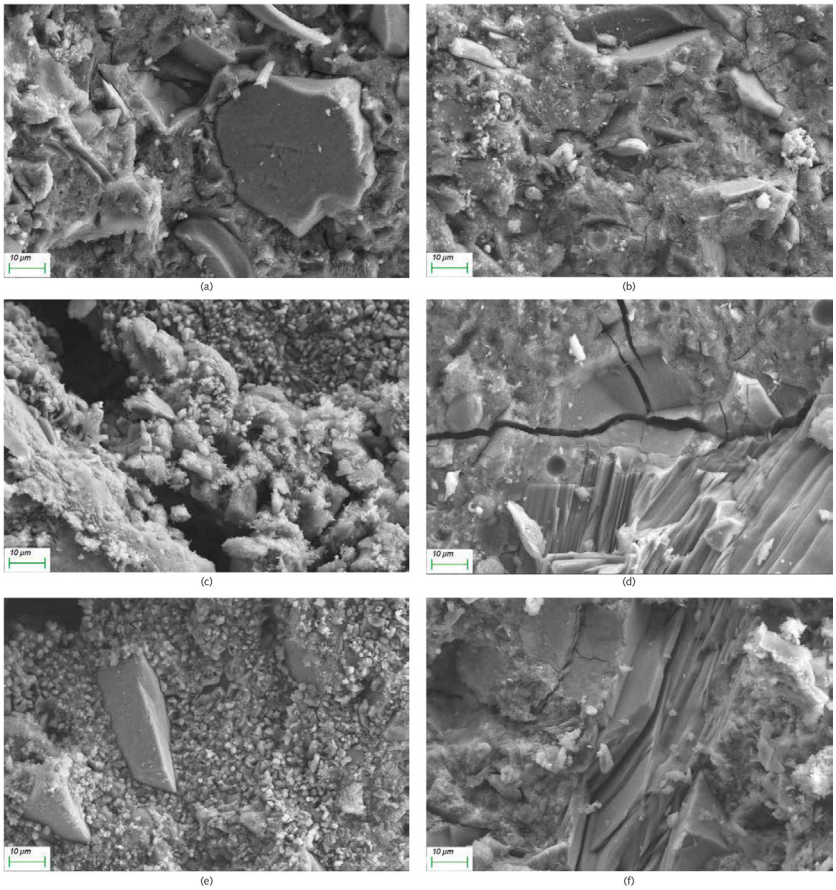

11 SEM images of A1 specimen with different erosion modes (a) A1-U 30 d (b) A1-U 120 d (c) A1-H 30 d (d) A1-H 120 d (e) A1-A 30 d (f) A1-A 120 d

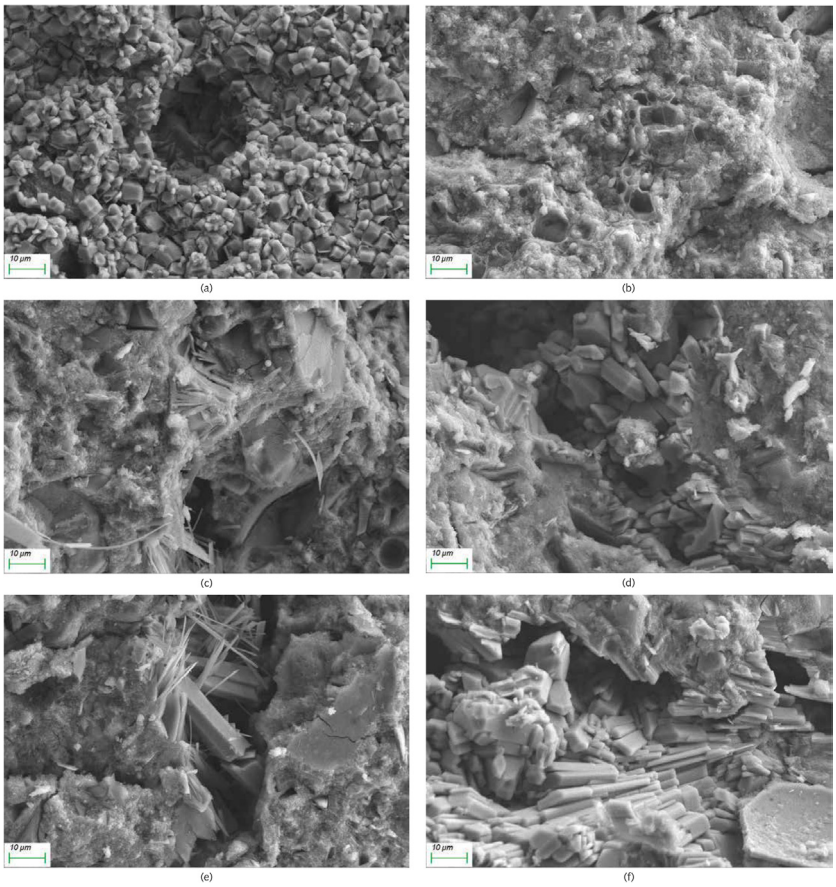

12 **SEM images of B2 specimens with different erosion modes (a) B2-U 30 d; (b) B2-U 120 d (c) B2-H 30 d; (d) B2-H 120 d (e) B2-A 30 d; (f) B2-A 120 d**

environments is covered with many gel materials with dense structure, and chemical erosion products such as gypsum are observed in the cracks. When the erosion age reaches 120 d, the surface becomes denser under water curing, and a large amount of gypsum formation is observed under both half-immersion and all-immersion environments, probably because the reaction of SO_4^{2-} in the sulfate solution with Ca^{2+} in the material, which is also consistent with XRD results.

4 Conclusion

(1) The mix ratio can affect the sulfate resistance of alkali-activated cementitious materials in the ternary system. The overall mechanical performance is better when 50% slag powder is added. The alkali-activated cementitious material containing 50% slag powder, 25% fly ash and 25% metakaolin shows excellent sulfate resistance in ammonium sulfate and the alkali-activated cementitious material containing 60% slag powder, 28% metakaolin and 12% fly ash has the worst corrosion resistance to ammonium sulfate.

(2) The results of XRD and SEM confirm the existence of the gypsum phase in alkali-activated cementitious materials specimens when exposed to ammonium sulfate, indicating that chemical erosion damage occurs in the interior. SEM images show that the alkali-activated cementitious materials of ternary mixture can form very dense microstructure and narrow micro cracks under sulfate attack.

(3) The alkali-activated cementitious materials in the ternary system show good resistance to sulphate attack under half-immersion, and its maximum compressive corrosion resistance coefficient can reach 1.28 at 120 d.

5 Acknowledgement

Financial supports from “The 14th Five Year plan” Hubei Provincial advantaged characteristic disciplines (groups) project of Wuhan University of Science and Technology (2023D0503; 2023D0501) and the State Key Laboratory of Silicate Materials for Architectures (Wuhan University of Technology) (SYSJJ2022-20) are gratefully acknowledged.

REFERENCES

[1] Zhang, H.Y.; Venkatesh, K.; Wu, B., et al.: Thermal behavior and mechanical properties of geopolymer mortar after exposure to elevated temperatures [J]. Construction and Building Materials, 2016, 109: pp. 17-24
[2] Yang, D.; Lu, M.Y.; Song, D., et al.: Research progress of geopolymer cement [J]. Materials Review, 2021, 35 (S1): pp. 644-649
[3] Gan, L.; Wu, J.; Shen, Z.Z., et al.: Deterioration law of basalt fiber reinforced concrete under sulfate attack and dry-wet cycle [J]. China Civil Engineering Journal, 2021, 54 (11): pp. 37-46
[4] Nuaklong, P.; Vanchai, S.; Prinya, C.: Properties of metakaolin-high calcium fly ash geopolymer concrete containing recycled aggregate from crushed concrete specimens [J]. Construction and Building Materials, 2018, 161: pp. 365-373
[5] Fu, B.; Cheng, Z.Y.; Han, J.Y., et al.: Strength and fresh properties of alkali-activated metakaolin slag geopolymer mortar [J]. Bulletin of the Chinese Ceramic Society, 2019, 38 (12): pp. 4013-4020
[6] Ismail, I.; Bernal, S.A.; Provis, J.L., et al. Microstructural changes in alkali activated fly ash/slag geopolymers with sulphate exposure [J]. Materials and Structures, 2013, 46 (3): pp. 361-373
[7] Atahan, H.N.; Dikme, D.: Use of mineral admixtures for enhanced resistance against sulfate attack [J]. Construction and Building Materials, 2011, 25 (8): pp. 3450-3457
[8] Irassar, E.F.; Maio, A.D.; Batic, O.R.: Sulfate attack on concrete with mineral admixtures [J]. Cement and Concrete Research, 1996, 26 (1): pp. 113-123
[9] Zheng, Y.; Wang, A.G.; Liu, K.W., et al.: Sulfate resistance and mechanism analysis of different geopolymer mortars [J]. Journal of Building Materials, 2021, 24 (6): pp. 1224-1233
[10] Nuaklong, P.; Vanchai, S.; Prinya, C.: Properties of metakaolin-high calcium fly ash geopolymer concrete containing recycled aggregate from crushed concrete specimens [J]. Construction and Building Materials, 2018, 161: pp. 365-373
[11] JGJ 63-2006. Standard of water for concrete [S]. Beijing/China
[12] GB/T 749-2008. The method for determing capability of resisting sulfate corrode of cement [S]. Beijing/China
[13] GB/T 17671-2021. Method of testing cements–Determination of strength [S]. Beijing/China
[14] Yang, Y.H.; Cong, B.R.; Guo, B.L., et al.: Study on properties of cement-based UHPC based on MAA model [J]. Construction Technology, 2022, 51 (21): pp. 60-65
[15] Xie, Q.; Wie, J.X.; Wu, J., et al.: Study on the multi-species ionic transport in concrete and its influence on migration of SO42- [J]. Concrete, 2020, (8): pp. 72-78
[16] Aboulayt, A.; Souayfan, F.; Roziere, E., et al. Alkali-activated grouts based on slag-fly ash mixtures: From early-age characterization to long-term phase composition [J]. Construction and Building Materials, 2020, 260: pp. 120510
[17] John, L.P.; Rupert, J.M.; Claire, E.W., et al. X-ray microtomography shows pore structure and tortuosity in alkali-activated binders [J]. Cement and Concrete Research, 2012, 42 (6): pp. 855-864